sustainability

MDPI

Article

Synthesis and Characterization of the Carbonate Hydrotalcites (NiAl-HT, CoAl-HT, and NiCoAl-HT), and Its Application for Removal of the Anionic Azo Dye Titan Yellow from Aqueous Solution

Samira Chouikh [1], Sabrina Cheikh [2], Ali Imessaoudene [2], Lotfi Mouni [2,*], Abdeltif Amrane [3,*], Amine Benahmed [1] and Noureddine Bettahar [1]

[1] Laboratoire De Chimie Des Matériaux Inorganiques Et Application (LCMIA), Faculté De Chimie, Université des Sciences Et De La Technologie d'Oran (USTO M. B), BP 1505, Oran 31000, Algeria; samira.chouikh@univ-usto.dz (S.C.); amine.benahmed@univ-usto.dz (A.B.); nbettahar2001@yahoo.fr (N.B.)

[2] Laboratoire de Gestion et Valorisation des Ressources Naturelles et Assurance Qualité, Faculté SNVST, Université de Bouira, Bouira 10000, Algeria; chikhsabrina@yahoo.fr (S.C.); a.imessaoudene@univ-bouira.dz (A.I.)

[3] Ecole Nationale Supérieure de Chimie de Rennes, Université de Rennes, CNRS, ISCR-UMR6226, 35000 Rennes, France

* Correspondence: l.mouni@univ-bouira.dz (L.M.); abdeltif.amrane@univ-rennes1.fr or abdeltif.amrane@univ-rennes.fr (A.A.)

Abstract: This work focuses on studying the removal of Titan Yellow (TY) dye, which is a water pollutant using three matrices of layered double hydroxide (LDHs; M^{+2}Al-HT), with M^{+2} = Ni, Co, or NiCo were synthesized using the co-precipitation technique in a solution with a constant pH. The X-ray diffraction (XRD) pattern of the formed solids shows that the synthesized phase is the LDH type with the average interlamellar distance ($\mathbf{d}_{spacing} \approx 7.595$ Å). The Fourier-transform infrared spectroscopy (FT-IR) spectra were compared, before and after adsorption, confirming the displacement of the carbonated interlayers and confirmed the presence of the S=O bond in the dye under study. Thermogravimetric-differential thermal analysis (TG/DTG) shows temperatures of decarbonation of the LDHs. The BET specific surface areas of NiAl-HT, NiCoAl-HT, and CoAl-HT were found equal to 156.819 $m^2 \cdot g^{-1}$, 142.72 $m^2 \cdot g^{-1}$, and 56.98 $m^2 \cdot g^{-1}$, respectively, and the SEM-EDX micrographs results confirmed the creation of the hydrotalcite type material. The UV–visible study of the adsorption of TY is performed by varying different parameters such as pH of the solution, mass, contact time, and temperature. The obtained isotherms from this kinetic study show that the adsorption of TY dye is more efficient in NiAl-HT. It can, therefore, be stated that the adsorption process of TY is endothermic and spontaneous. The results of this study could be extended to other anionic azo dyes having similar chemical structures.

Keywords: carbonate hydrotalcites; co-precipitation; characterization; adsorption; titan yellow

check for updates

Citation: Chouikh, S.; Cheikh, S.; Imessaoudene, A.; Mouni, L.; Amrane, A.; Benahmed, A.; Bettahar, N. Synthesis and Characterization of the Carbonate Hydrotalcites (NiAl-HT, CoAl-HT, and NiCoAl-HT), and Its Application for Removal of the Anionic Azo Dye Titan Yellow from Aqueous Solution. *Sustainability* **2023**, *15*, 7948. https://doi.org/10.3390/su15107948

Academic Editor: Ismat Hassan Ali

Received: 3 April 2023
Revised: 4 May 2023
Accepted: 9 May 2023
Published: 12 May 2023

Copyright: © 2023 by the authors. Licensee MDPI, Basel, Switzerland. This article is an open access article distributed under the terms and conditions of the Creative Commons Attribution (CC BY) license (https://creativecommons.org/licenses/by/4.0/).

1. Introduction

It is widely admitted that water has always been considered as the most important component of life for all living creatures. With the ever-increasing global warming and desertification, water scarcity is progressively becoming a serious threat for most countries around the world [1,2]. Today, water shortage is viewed as a highly critical issue that is unfortunately getting worse day after day. In addition, this scarce resource is continuously exposed to pollution by synthetic chemicals that are widely used in several industrial applications of dyes [3,4].

It is worth indicating that dyes can contaminate important amounts of water even when released in very small quantities (1 ppm). It has been reported that huge amounts of

dyes are produced annually (7×10^5 tons/year). Reports have indicated that 2% of that quantity is directly discharged into the aquatic ecosystem, and 10% of textile dyes are lost during the dyeing, tanning, and finishing processes, which means that water pollution is an issue that ought to be faced seriously [5]. Moreover, dyes generally exhibit mutagenic, teratogenic, and carcinogenic effects and can therefore engender various health disorders to human beings. They can indeed have serious adverse effects on the functioning of several organs like the central nervous system, liver, brain, kidney, and reproductive system [6]. Among these dyes, azo dyes are considered the most persistent and dangerous industrial pollutants due to their ability to contaminate natural water. They are the most utilized dyes, accounting for more than 60% of all commercially available dyes [7]. Among the azo dyes, Titan Yellow (TY), also called Thiazole Yellow and Clayton Yellow, as shown in Figure 1, is a negatively charged azo dye molecule with sulfonic groups [8]. TY in wastewater can destroy the water ecosystem and be harmful to human health. TY is selected in this study because of its complex chemical structure (pka = 12.1), high solubility in aqueous solution, widespread application, and its persistence once it is discharged into environment [9]. So far, only a few preliminary studies have been conducted about a treatment method for the removal of this target pollutant (TY).

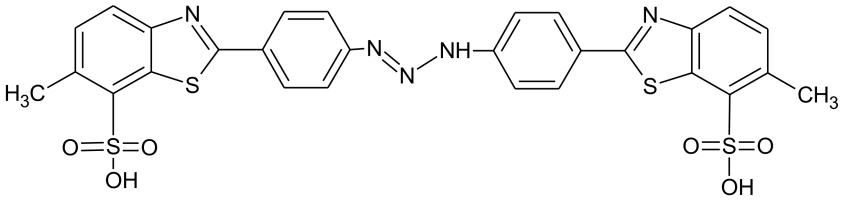

Figure 1. Chemical structure of Titan Yellow (TY). In general, dyes are dangerous for human beings and therefore their removal from all kinds of effluents is more than essential and urgent. Fortunately, a number of techniques, such as coagulation/flocculation [10], photocatalytic degradation [11], ozonation [12], ion exchange [13], biological processes [14], and adsorption [15], can be used to effectively remove dyes from contaminated effluents. It has been revealed that adsorption is one of the most effective methods for the removal of dyes from wastewaters. This technique has many benefits as it consumes small amounts of energy, is easy to apply, and is cost-effective [16]. It should be noted that different types of adsorbents are available today. In addition to the activated carbon [17], zeolite [18], metal oxides or hydroxides [19], and calix [20], adsorbents obtained from various sources, including agricultural wastes [21], hydroxyapatite derived from food industry bio-wastes [22], fly ash from industries [23], aquatic plants [24–26], vegetable and fruit wastes [27,28], and many others have been demonstrated to be promising and effective alternatives.

Over the last few decades, layered double hydroxides (LDHs), also known as hydrotal cite-like compounds (HT), have received an increasing interest from researchers for the purpose of adopting them in environmental remediation processes [29,30] that use ionophore-like compounds in potentiometric sensors and biosensors [31]. LDHs have many physical and chemical properties that are surprisingly similar to those of cationic clay minerals. Their layered structure, wide chemical composition (due to variable isomorphous substitution of metal cations), variable layer charge density, reactive interlayer space, swelling in water, rheological and colloidal properties, ion-exchange properties in relation to its layered structure for use in adsorption processes, and removal of anionic dyes give these materials significant efficiency and performance in this area [32]. The general formula of LDH is given as $[M^{2+}{}_{1-x}M^{3+}{}_x(OH)_2(A^{n-})_{x/n}]\cdot y(H_2O)$, where M^{2+} is a divalent metal cation (Ni, Co or NiCo which gives better results), M^{3+} is a trivalent metal cation, A^{n-} is an interlayer anion, x is the ratio of $M^{+3}/(M^{2+}+M^{+3})$, and y represents the number of water molecules. It should be noted that these quantities may vary over a wide interval, whereas A^{n-} can be exchanged with other anions quite easily [33]. Many researchers have shown that LDHs can adsorb some inorganic or organic pollutants through exchange with inter-layer anions. However, $CO_3{}^{2-}$ is preferentially attached and readily replaceable by other anions [34].

It was found that LDH materials can be prepared using different traditional techniques, including co-precipitation, urea hydrolysis, ion exchange, and hydrothermal synthesis [35]. Details of methods and conditions for the synthesis of various LDHs are shown in Table 1

Table 1. Details of methods and conditions for the synthesis of various LDHs.

Adsorbent LDH	Adsorbate	Method of Synthesis	Molar Ratio	pH	Ref
Cu-Al-CO_3	Evans Blue	Co-precipitation	2	10	[32]
Ni−Co LDH	SO_4^{2-}, HPO_4^{2-} NO^{3-}	flux method	-	-	[36]
Ni_2Al-CO_3 LDH (LDH) and Ni_2Al-CO_3 LDO (LDO)	Indigo Carmine Congo Red	Co-precipitation	2	10	[37]
Zn-Fe-CO_3 Zn-Cr-CO_3Zn-Al-CO_3	Indigo Carmine	Co-precipitation	2	7	[38]
Zn-Al-Fe	Phosphate P(V) and chromate Cr (VI)	Co-precipitation	2/0.5/0.5	10	[39]
Mg/Al HT	Navy Blue Yellow F3G	Co-precipitation	-	-	[40]
Mg-Al-CO_3-LDH	Acid Yellow 42	Co-precipitation	-	10	[34]
Ni/Zn/Fe-LDH	Reactive Black 5 RB5	Co-precipitation	0.5/1/1	10	[41]

This study seeks mainly to assess the adsorption efficiency of the carbonate hydrotalcite (HT; $M^{+2}M^{3+}$-HT), with M^{+2} = Ni, Co or NiCo: (NiAl-HT, CoAl-HT, NiCoAl-HT), M^{3+} = Al and HT are CO_3 in removing the anionic azo dye Titan Yellow from effluents. For this, it was decided to carry out a detailed investigation of the impact of different sorption factors, that is, the solution pH, adsorbent masse, contact time, and temperature, in order to identify the adsorption performance of these materials under optimized conditions. In addition, kinetic representations, like the pseudo-first-order representation, pseudo-second-order representation, and intraparticle diffusion, as well as equilibrium isotherms and thermodynamic parameters, were used to describe the adsorption process.

2. Materials and Methods

2.1. Chemicals and Materials

The chemical reagents $N_iCl_2{\cdot}6H_2O$ (97%), $AlCl_3.6H_2O$ (97%), NaOH (97%), Na_2CO_3 (99.8%), $CoN_2O_6{\cdot}6H_2O$ (99%), and HCl (36%), were all purchased from Biochem Chemopharma, Cosne-Cours-sur-Loire, France. The empirical formula of Titan Yellow (99%) (disodium 2, 2′-[(1E)-triaz-1-ene-1, 3-diyldibenzene-4, 1-diyl] bis (6-methyl-1, 3-benzothiazole-7sulfonate) is $C_{28}H_{19}N_5Na_2O_6S_4$, and its molecular weight is 695.71 $g{\cdot}mol^{-1}$. This dye was also supplied by the same manufacturer. It is worth emphasizing that distilled water was employed throughout all the steps of the synthesis process.

2.2. NiAl-HT, CoAL-HT, and NiCoAL-HT Synthesis

The co-precipitation method [38] is used to synthesized the three phases NiAl-HT, CoAL-HT, and NiCoAL-HT at temperature (T = 25 °C), with a molar ratio R = (M^{2+}/M^{3+}) = 2 and a constant pH.

Next, samples of NiAl-HT and CoAL-HT were co-precipitated by adding, drop wise, 50 mL of a solution containing 2 moles of $NiCl_2{\cdot}6H_2O$ or $CoN_2O_6{\cdot}6H_2O$ and 1 mole of $AlCl_3{\cdot}6H_2O$ to 50 mL of an aqueous solution including 2 moles of Na_2CO_3 and 1 mole of NaOH. The mixture was stirred by a magnetic stirrer (IKA, RH Basic KT/C, Teltow, Germany) at 200 rpm for 360 min.

Regarding the sample NiCoAL-HT, it was co-precipitated by adding, drop wise, 50 mL of a solution containing 1 mole of $NiCl_2{\cdot}6H_2O$, 1 mole of $CoN_2O_6{\cdot}6H_2O$, and 1 mole of $AlCl_3{\cdot}6H_2O$ to 50 mL of an aqueous solution containing 2 moles of Na_2CO_3 and 1 mole of NaOH. The mixture was stirred by a magnetic stirrer at 200 rpm for 360 min. Note that the

pH value of the resulting solution was kept constant at 9.8 by adding appropriate amounts of a 1 M NaOH solution measured by a pH meter (Mettler Toledo, Columbus, OH, USA). Finally, the suspension obtained was hydrothermally processed by heating in an oven at 70 °C (Memmert GmbH + Co. KG, Bavaria, Germany) for 24 h and then centrifuged, washed several times, and dried at 80 °C for 24 h.

2.3. Characterization

The X-ray diffraction (XRD) technique was employed for the characterization of the NiAl-HT, CoAl-HT, and NiCoAl-HT using an X Pert Pro X-ray diffractometer, supplied by PANalytical, operating at 45 KV and 40 mA, over a 2θ range (5° to 70°), with λ = 1.5406 Å and an accuracy of 0.02°.

As for the FTIR spectra, they were recorded within the interval extending from 4000 to 400 cm^{-1} using a Bruker ATR-diamant-type device and KBr pellets. Moreover, the thermogravimetric analysis (TGA/DTG) was performed in order to estimate the mass variation of each sample as a function of temperature. This technique can also be used for monitoring the evolution of the chemical composition of solids during their calcinations. Note also that a SETARAM MTB thermobalance with a sensitivity of 10^{-8}g was used in this case. In this thermal analysis technique, the sample is often placed in an alumina container or crucible, and calcined from 25 °C to 700 °C, at 10 °C·min^{-1}.

Afterwards, the specific surfaces of the samples were determined by the (BET) approach using a Quantachrome Nova 3200 e type surface analyzer. With regard to degassing, it was carried out before conducting the analysis in order to remove the humidity within the adsorbent pores. It should be known that each sample was processed under vacuum at a temperature equal to 100 °C for a period of 8 h. The temperature was increased at a fixed rate of 3 °C·min^{-1}. After activation, the tubes containing the samples were immersed in a liquid nitrogen bath, and then nitrogen gas was injected at different pressures. In addition, the pore diameter was determined by the BJH method [42]. Scanning electron microscopy (SEM) was accomplished to observe the surface morphology of the samples using a JSM-IT300 instrument and X-ray energy dispersion (EDX) analysis at accelerating voltage of 20 KV to approve the elemental composition of the materials.

A scan was performed within the wavelength range between 250 and 600 nm using a UV–visible spectrophotometer (Shimadzu UV 1700, Japan) to dye solutions at natural pH. Subsequently, a calibration curve was drawn at maximum absorbance (λ_{max} = 400 nm). The residual dye concentrations after each adsorption test were determined from this curve.

To determine the point of zero charge pH (PZC) of the materials, the "drift method" was applied [43]: 0.2 g of adsorbent was added to 40 mL of the 0.1 mol/L NaCl solution at different initial pH values (pH_i) in the range of 3–12, and agitated for 24 h at room temperature; the final pH (pH_f) values of solutions were then measured, and ΔpH is plotted vs. pH_i.

2.4. Adsorption Procedure

Classical batch adsorption investigations were carried out for the purpose of evaluating the sorptive properties of NiAl-HT, CoAl-HT, and NiCoAl-HT. For this purpose, a dye stock solution of TY1000 mg·L^{-1} was prepared. Then, the desired concentration was obtained through dilution. Moreover, parameters, like dye solution pH, the adsorbent masse, contact time, and temperature which may affect the adsorption capacity of our solid samples, were investigated.

It is worth emphasizing that all adsorption experiments were conducted in 100 mL conical flasks at room temperature (except in the study of the effect of temperature), using a volume of 20 mL of TY with an initial concentration of 100 mg·L^{-1} (unless otherwise indicated) with a determined mass of the adsorbent. The mixture was subjected to magnetic stirring during 180 min at 200 rpm. Once the adsorption experiment was finished, the separation solid–liquid was spun at 6500 rpm for 10 min in a centrifuge (Eppendorf model

5702, Hamburg, Germany). Finally, the residual dye concentrations were determined using a UV–Visible spectrophotometer.

The amount of dye adsorbed on an adsorbent surface at equilibrium Q_e ($mg \cdot g^{-1}$)and dye removal efficiency E (%) were evaluated using Equations (1) and (2) [44].

$$Q_e = (C_i - C_e)\frac{V}{m} \quad (1)$$

$$E(\%) = \frac{(C_i - C_e)}{C_i}100 \quad (2)$$

where C_i and C_e are, respectively, the initial and equilibrium concentrations ($mg \cdot L^{-1}$), m (g) is the mass of adsorbents, and V (L) is the volume of solution.

2.4.1. Effect of Initial pH

A mass of 80 mg of our adsorbents (NiAl-HT, CoAl-HT, NiCoAlL-HT) was added to 20 mL of the dye solutions (100 $mg \cdot L^{-1}$) with an initial pH values adjusted from 3 to 11 by using either HCl (1 N) or NaOH (1 N) as required. The obtained suspensions were shaken for 24 h to ensure that the systems have reached a steady-state or pseudo-equilibrium.

2.4.2. Effect of Adsorbent Mass

Different masses of carbonate clays of NiAl-HT, CoAl-HT, and NiCoAl-HT were used to test their effectiveness in dye uptake. For this, volumes of 20 mL of the TY solution (pH 3), with initial dye concentrations of 100 $mg \cdot L^{-1}$, were brought into contact with specific masses of the above materials between 10 mg and 100 mg. The contact time was set to 180 min, and then the residual TY concentrations were analyzed.

2.4.3. Effect of Contact Time

In this section, adsorption kinetic studies were carried out on a dye solution using the previously solids samples. This study was conducted at room temperature, by contacting the dye solutions (100 $mg \cdot L^{-1}$) at pH 3 with different adsorbents at a dose of 4 $g \cdot L^{-1}$.The mixture was put under continuous stirring at 200 rpm. Samples of 3 mL were withdrawnfrom the mixture at different times.

2.4.4. Effect of Temperature

This section aims to examine the effect of temperature on TY uptake onto the solid sorbents NiAl-HT, CoAl-HT, and NiCoAl-HT within the temperature range extending from 298 to 328 K. The adsorption process was examined at different temperatures, under optimum adsorption conditions of the sorbents, and using the optimized parameters for the sorbent amount, solution pH 3, initial concentration = 100 $mg \cdot L^{-1}$, and contact time.

3. Results and Discussion

3.1. Characterization of NiAl-HT, CoAl-HT, and NiCoAl-HT

Figure 2 depicts the XRD patterns of the samples NiAl-HT, CoAl-HT, NiCoAl-HT. The reflections corresponding to the sharp peaks indicate that the concerned sample has a crystalline structure, which is typical of hydrotalcite-like materials. All these samples exhibited a high crystallinity level as a result of the synthesis conditions used (slow addition, ageing). The presence of amorphous α-Ni $(OH)_2$, β-Co $(OH)_2$, and Co $(OH)_3$ cannot be ignored in the XRD pattern of NiCoAl-HT [45]. This is certainly due to the inadequate control of the pH level during the synthesis [38].

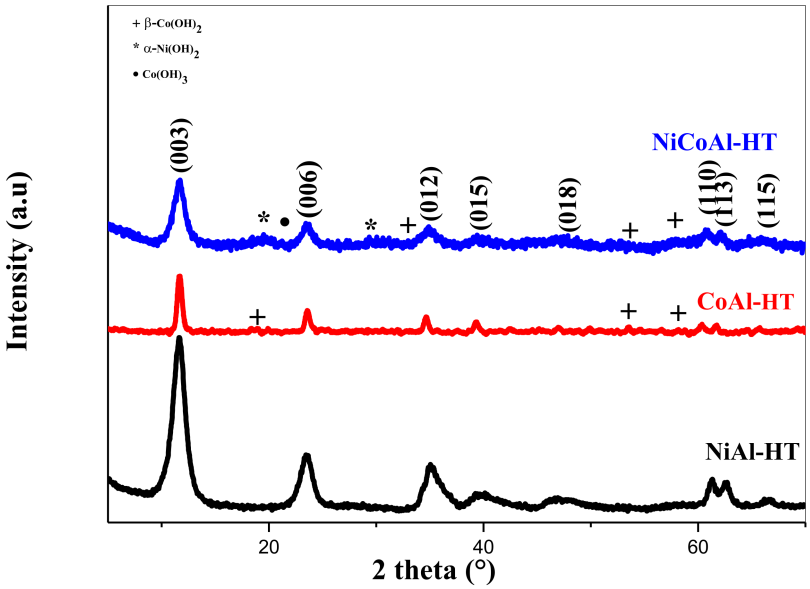

Figure 2. XRD patterns of: NiAl-HT, CoAl-HT, and NiCoAl-HT LDHs.

Furthermore, the above structure crystallized in the hexagonal space group R3m (three-layer polytype) and the diffraction peaks were found to correspond to the sharp and symmetric peaks for the (003), (006), and (012) crystallographic planes and the broad and asymmetric peaks for the (015), (018), (110), (113), and (115) crystallographic planes. It should also be noted that the interlayer space corresponding to $\mathbf{d}_{003}$ mainly depends on the size of the intercalated anion. It was evaluated at 7.621 Å, 7.568 Å, and 7.597 Å for NiAl-HT, CoAl-HT, and NiCoAl-HT, respectively. In addition, the average interlamellar distance ($\mathbf{d}_{spacing} \approx 7.595$ Å) was found to be in accordance with the presence of intercalated carbonate anions [33].

The value of the cell parameter **a** was calculated from the position of the (1 1 0) reflection ($\mathbf{a} = 2\ \mathbf{d}_{110}$). This parameter corresponds to the average distance between the two nearest metal cations within the hydroxide layers, whereas the cell constant **c** is generally evaluated as $\mathbf{c} = 3\mathbf{d}_{003}$. The results reported in Table 2 show that there is a minor decrease in the LDH lattice parameter **a**, which is most likely due to the difference between the ionic radii of ions Ni^{2+} (0.69 Å) and Co^{2+} (0.65 Å) which are larger than that of Co^{3+} (0.545 Å) [38]. The decrease in the peak intensity for the (110) plane was found in the order: NiAl-HT, NiCoAl-HT, and CoAl-HT, which means that the crystallinity dropped [38].

Table 2. Interlamellar distance ($\mathbf{d}_{003}$) and cell parameters (a,c) of LDHs derived from X-ray diffraction patterns.

LDHs	d003 (Å)	a (Å)	c (Å)
NiAl-HT	7.621	3.021	22.864
NiCoAl-HT	7.597	3.044	22.791
CoAl-HT	7.568	3.018	22.704

The FTIR spectra of NiAl-HT, CoAl-HT, and NiCoAl-HT as well as those of NiAl-TY, CoAl-TY, and NiCoAl-TY, after adsorption, are clearly displayed in Figure 3. Based on studies available in the literature, these spectra exhibit a profile that is similar to that of hydrotalcites [33]. It should also be mentioned that broad, antisymmetric bands centered around 3439, 3440, and 3350 cm^{-1} for NiAl-HT, CoAl-HT, and NiCoAl-HT, respectively, and relating to the stretching modes of the hydroxyl groups, both from the layer groups and from the interlayer water molecules, in addition to those adsorbed on the external surface of the crystallite [46]. Further, medium intensity bands, centered at 1634,1650, and 1626 cm^{-1}, corresponding to NiAl-HT, CoAl-HT, and NiCoAl-HT, respectively, were

certainly due to the deformation of the interlayer water molecules. In addition, a strong band was observed around 1350 cm^{-1} for all samples. This may be attributed to the weak band that was revealed at 1100 cm^{-1} and to the presence of carbonate ions. Moreover, the shoulders at 849, 857, and 930 cm^{-1} and the bands at 719, 711, and 776 cm^{-1} for NiAl-HT, CoAl-HT, and NiCoAl-HT, were, respectively, due to the M-OH deformation and translation modes [47–49]. Furthermore, the characteristic adsorption bands of our samples after TY adsorption can easily be evidenced in the spectra of NiAl-TY, CoAl-TY, and NiCoAl-TY. Note also that the asymmetric stretching vibration that is associated with the S=O bonding appears around 1100 cm^{-1} [47]. It is interesting to mention another band located around 1700 cm^{-1}; this band is indicative of the vibrations of the C=C bonds in the aromatic ring [50], which confirms the presence of the TY dye ions that were adsorbed on these three materials. Moreover, the band characteristic of the carbonate anion was evidenced by the fact that the intensity of the spectra of NiAl-TY, CoAl-TY, and NiCoAl-TY was smaller than that of NiAl-HT, CoAl-HT, and NiCoAl-HT, which shows that the interlayer carbonate anions were, displaced [38].

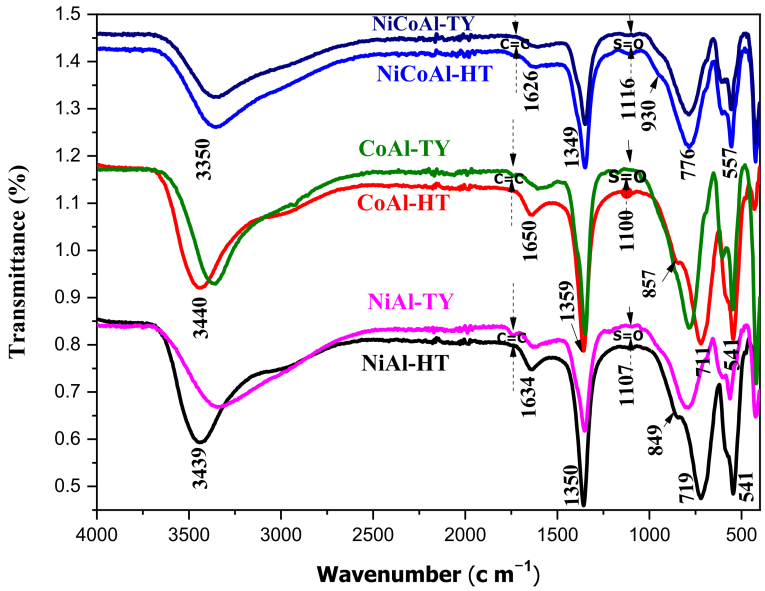

Figure 3. FTIR patterns of NiAl-HT, CoAl-HT, and NiCoAl-HT (before TY adsorption), NiAl-TY, CoAl-TY, and NiCoAl-TY (after TY adsorption).

The (DTG/TG) thermograms of the NiAl-HT, CoAl-HT, and NiCoAl-HT materials are clearly represented in Figure 4. A close examination of the TG curves suggests the existence of three mass loss stages for all samples. Similarly, the DTG profiles confirm the existence of three endothermic peaks.

The first stage, that is, first weight loss, corresponds to a band located between 25 °C and 120 °C, corresponding to the first endothermic peak that represents 8.32%, 2.04%, and 9.12% for NiAl-HT, CoAl-HT, and NiCoAl-HT, respectively. This weight loss may be assigned to the loss of nonstructural water that was adsorbed on the external surface of the hydrotalcite crystals. The second stage occurs between 120 °C and 290 °C for NiAl-HT and NiCoAl-HT, whereas it is between 120 °C and 260 °C for CoAl-HT. This phase corresponds to the loss of intercalated water; it may be ascribed to the second DTG peak, which corresponds to 10.34%, 2.71%, and 7.57% for NiAl-HT, CoAl-HT, and NiCoAl-HT, respectively. The third and last stage takes place in the vicinity of 400 °C for NiAl-HT and NiCoAl-HT, whereas it occurs between 260 °C and 300 °C for CoAl-HT; this phase is equivalent to the decomposition of the hydroxyl groups and carbonate anions, which leads to the release of CO_2 that is associated with the third endothermic DTG peak; this represents 17.51%, 23.11%, and 15.28 % for the above samples [31].

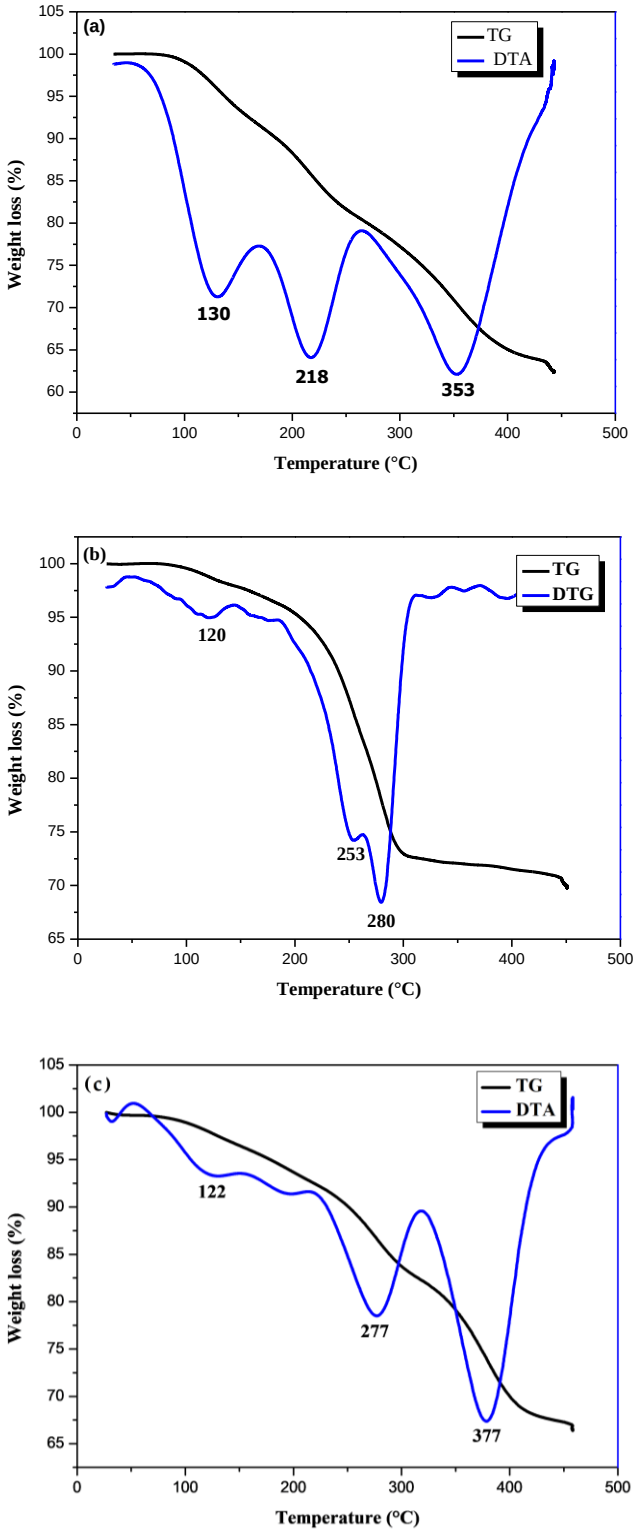

Figure 4. TG/DTG profiles of: (**a**) NiAl-HT, (**b**) CoAl-HT, and (**c**) NiCoAl-HT.

It was also observed that the weight loss due to the interlayer water (10.34%) of the sample NiAl-HT is more important than that of the other compounds (around 2.71% and 7.57%); this is probably because the ionic radii of the studied elements are different which can lead to differences in the structural properties of the resulting material.

The presence of a high content of water molecules in this sample generated a slight increase in the interfoliar distance which makes it a potential material for the elimination

of organic pollutants. Thus, a material having a hydrophilic character can be used as an effective material for the elimination of hydrophilic pollutants, which is the case of the NiAl-HT sample.

The FTIR spectra presented in Figure 3 show that the bands corresponding to the range 3700–3500 cm^{-1} and the bending vibrations (around 1630 cm^{-1}) of the interlayer water are more intense in NiAl-HT than in the other samples, which implies that this sample contains a higher amount of interlayer water.

Nitrogen adsorption/desorption isotherms obtained are presented in Figure 5. Isotherms shapes exhibit type IV with H3 hysteresis loop based on the IUPAC classification [51]. The results forms indicating the domination of mesoporous structure of all adsorbents. The NiAl-HT sample present a highest BET surface equal to 156.819 $m^2 \cdot g^{-1}$ and a highest average pore size radius equal to 36.054 nm. However, the pore volume presents an inverse trend; NiAl-HT pore volume equal to 0.283 $cm^3 \cdot g^{-1}$ is lower than CoAl-HT and NiCoAl-HT. This discordance can be attributed to the condensation on mesoporous pores at pressure near to $P/P_0 = 1$. The detailed textural parameters are listed in Table 3.

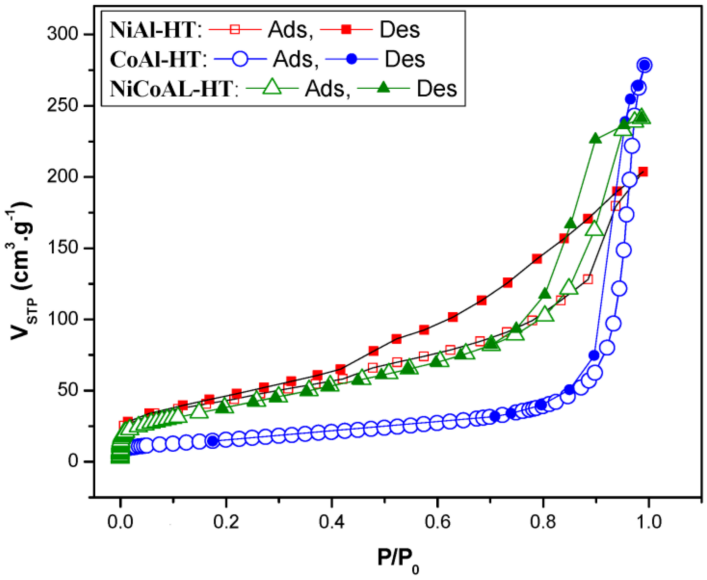

Figure 5. N_2 adsorption-desorption isotherms of: NiAl-HT, CoAl-HT, and NiCoAl-HT.

Table 3. Specific surface area (S_{BET}), pore volume (V_p), and average pore size radius for NiAl-HT, CoAl-HT, and NiCoAl-HT.

Sample	Specific Surface Area SBET ($m^2 \cdot g^{-1}$)	Pore Volume Vp ($cm^3 \cdot g^{-1}$)	Average Pore Size Radius (nm)
NiAl-HT	156.819	0.283	36.054
CoAl-HT	56.98	0.406	22.769
NiCoAl-HT	142.72	0.369	13.132

SEM micrographs of NiAl-HT, CoAl-HT, and NiCoAl-HT are presented in Figure 6a–c, respectively. The image indicates that the three hydrotalcites have platelet morphology with a smooth surface and a regular shape of the grains.

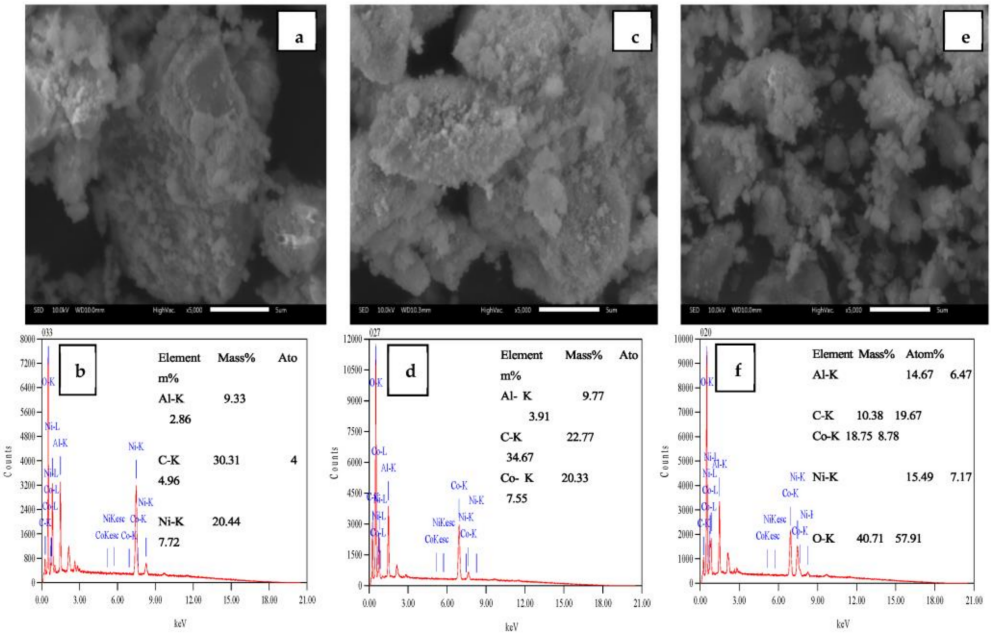

Figure 6. SEM images and EDX analysis of NiAl-HT (**a**,**b**), CoAl-HT (**c**,**d**), NiCoAl-HT (**e**,**f**).

The EDX spectrum of NiAl-HT, CoAl-HT, and NiCoAl-HT shown in Figure 6d–f indicate the presence of aluminum, carbon, nickel, cobalt, and oxygen. The molar ratios of Ni/Al, Co/Al, and (Ni + Co)/Al were found to be 2.19, 2.08, and 2.33, respectively, which is in good agreement with the ratio of 2 used in the preparation. These results confirm the creation of the hydrotalcite type material.

3.2. Adsorption Study of Titan Yellow

3.2.1. Effect of Initial pH

The results of the influence of the initial dye solution pH, investigated between 3 and 11 on the adsorption capacities of the different adsorbents is presented in Figure 7a. This figure shows that the TY uptake is relatively important at pH 3. The Qe values obtained at this point are 28.2, 26.5, and 24.4 $mg \cdot g^{-1}$ for NiAl-HT, NiCoAl-HT, and CoAl-HT, respectively. The analysis of these results with respect to the pH zero charge pH (Pzc) values of the materials (Figure 7b) which are very similar and close to pH 9.5 indicate that, at pH lower pH (PZC), the surface charge of the materials is positive; however, it is negative at higher pH. Taking into account that TY is an anionic dye, an electrostatic interaction is favorable at pH 3 between the materials surfaces and the dye molecules. The fact that the carbonate anions can be liberated from the materials matrix as CO_2. It was indeed found that the conversion rate of carbonate anions to CO_2 is higher at low solution pH than at high solution pH [32]. Therefore, at acidic medium, the dye adsorption process can takes place through two possible processes: anion exchange (Equation (3)) and reconstruction of the layered structure by rehydration (Equation (4)) [46].

$$\left[M^{2+}_{1-X}M^{3+}_{X}(OH)_2\right]A_X \cdot yH_2O + \frac{x}{n}X^{n-} \rightarrow \left[M^{2+}_{1-X}M^{3+}_{X}(OH)_2\right]X_{\frac{x}{n}} \cdot yH_2O + A^- \quad (3)$$

$$\left[M^{2+}_{1-X}M^{3+}_{X}(OH)_2\right]A_X \cdot yH_2O + \frac{x}{n}X^{n-} \rightarrow \left[M^{2+}_{1-X}M^{3+}_{X}(OH)_2\right]X_{\frac{x}{n}} \cdot yH_2O + A^- \quad (4)$$

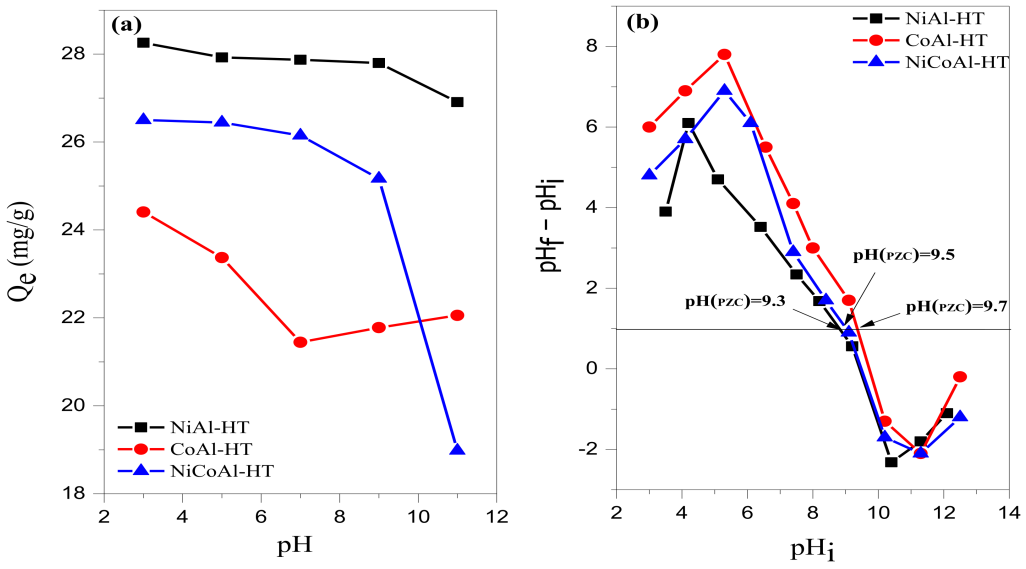

Figure 7. Effect of initial solution pH on TY uptake (C_0 = 100 mg·L^{-1}, m = 80 mg, V = 20 mL, T = 25 °C) (**a**), Zero point charge determination (**b**).

For this purpose, pH 3 of the dye solutions has been fixed for all other adsorption experiments.

3.2.2. Effect of Adsorbent Dose

The effect of adsorbent dose is an important parameter controlling the adsorption process. The removal efficiency (E) of TY in the different systems studied is illustrated in Figure 8. As can be seen from this figure, the removal of TY increased when the adsorbents amount increased, which could be attributed to the greater availability of sorptive sites; after reaching a plateau from the mass 80 mg, one can observe the steady-state of the (pseudo) equilibrium, likely because of the saturation of the available sites. For the following investigation a dose D of 4 g·L^{-1} has been chosen as the optimum value.

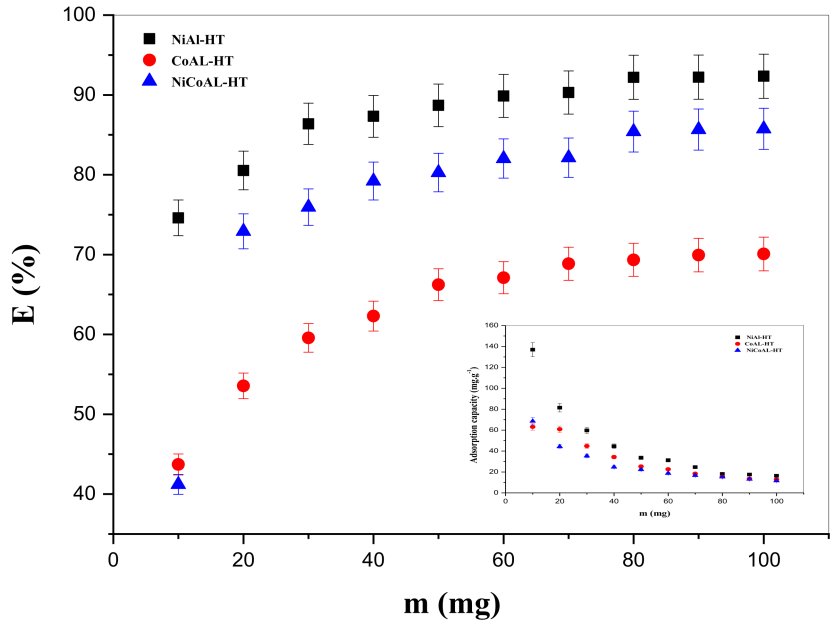

Figure 8. Removal efficiency of TY as a function of the mass of adsorbents NiAl-HT, CoAL-HT, and NiCoAl-HT and the adsorption capacity (C_i = 100 mg·L^{-1}, V = 20 mL, T = 25 °C).

3.2.3. Effect of Contact Time

Figure 9 depicts the evolution of the adsorption capacity of dye TY as the contact time increased. It has been revealed that the adsorption of organic compounds on clays takes place through two phases. The first phase is quite rapid, whereas the second one is slower [52]. Contact time has an effect on the amounts of dye adsorbed on carbonated materials. Indeed, it turned out that the adsorption capacity of TY dye increased over time until reaching equilibrium after 40 min, 90 min, and 120 min for, respectively, NiAl-HT, CoAl-HT, and NiCoAl-HT. This finding allowed concluding that the equilibrium time depends directly on the structures and chemical compositions of both the adsorbent and adsorbate [39]. It should be mentioned that the amount of dye adsorbed at equilibrium was 29.29 $mg{\cdot}g^{-1}$, 20.72 $mg{\cdot}g^{-1}$, and 24.30 $mg{\cdot}g^{-1}$ for NiAl-HT, CoAl-HT, and NiCoAl-HT, respectively, which is confirmed by the increased XRD interlayer spacing.

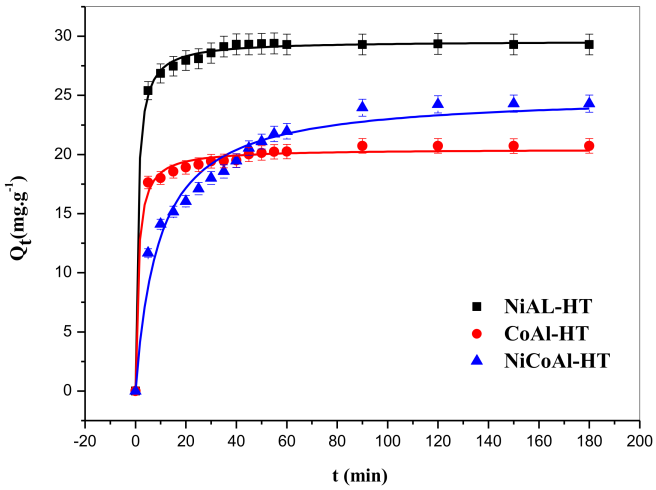

Figure 9. Non-Linear regression plots of Pseudo-second-order kinetic model for the adsorption of TY onto NiAl-HT, CoAl-HT, and NiCoAl-HT (C_i = 100 $mg{\cdot}L^{-1}$, pH = 3, D = 4 $g{\cdot}L^{-1}$, T = 25 °C).

3.2.4. Effect of Temperature

It turned out that the removal efficiency of titan yellow increases as the reaction temperature rises (Figure 10a). These observations may be explained by the fact that the mobility of dye ions increases due to the increase in the thermal energy of the adsorbents when temperature goes up [39].

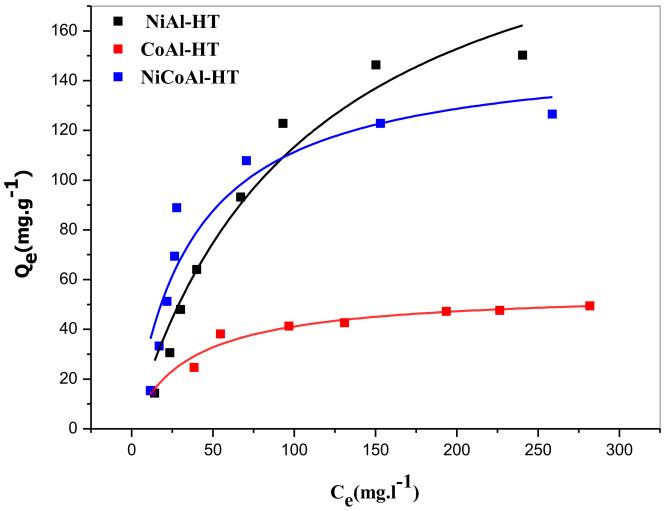

Figure 10. Non-Linear regression plot of the adsorption isotherm of TY dye onto NiAl-HT, CoAl-HT and NiCoAl-HT, according to the Langmuir model.

3.2.5. Kinetics Studies

Three kinetic models are generally used for monitoring and assessing the adsorption efficiency of an adsorbent. These are the pseudo-first-order kinetic models derived by Lagergren and represented by Equation (5), the pseudo-second-order kinetic model suggested by Ho and McKay and described by Equation (6), and the intra-particle diffusion kinetic model established by Weber and Morris and defined by Equation (7) [8].

$$Q_t = Q_e\left(1 - e^{K_1\ t}\right) \tag{5}$$

$$Q_t = \frac{Q_e^2\ K_2\ t}{1 + Q_e K_2 t} \tag{6}$$

$$Q_t = K_{int} t^{1/2} + C \tag{7}$$

Note that Q_e and Q_t are, respectively, the adsorption capacities ($mg{\cdot}g^{-1}$) at equilibrium and at time t, K_1 (min^{-1}), K_2 ($g{\cdot}mg^{-1}min^{-1}$), K_{int} ($mg{\cdot}g^{-1}{\cdot}min^{-1}$), and C ($mg{\cdot}g^{-1}$) are the pseudo-first-order adsorption rate constant, pseudo-second-order adsorption rate constant, intra-particle diffusion rate constant and the thickness of boundary layer of adsorbate on adsorbent sites, respectively. The parameters K_1, K_2, and Q_e were obtained for the sorption of TY onto NiAl HT, CoAL-HT, and NiCoAl-HT.

The fitting of the chosen models was evaluated by using nonlinear modeling performed, and the best-fitting model was identified using the coefficient of determination (R^2), the mean square error (MSE), and the root sum of square error (RMSE) statistic tests which can be calculated as the following Equations (8)–(10) [53]:

$$R^2 = 1 - \frac{\sum_1^n \left(Y_i - \hat{Y}_i\right)^2}{\sum_1^n \left(Y_i - \overline{Y}\right)^2} \tag{8}$$

$$MSE = \frac{\sum_1^n \left(Y_i - \hat{Y}_i\right)^2}{DF} \tag{9}$$

$$RMSE = \sqrt{MSE} \tag{10}$$

where (Y_i) is the experimentally obtained adsorption capacities, ($\overline{Y}$) is their mean, ($\hat{Y}_i$) is the model-predicted capacities, and (DF) is the degree of freedom.

As is clearly revealed in Figure 9 and Table 4, the adsorption process is well represented a nonlinear expression by the pseudo-second-order representation for all three adsorbents, with R^2 values close to unity. In addition, the RMSE and X^2 values are smaller than those of the pseudo-first-order model and intraparticle diffusion. Further, the Q_e values estimated by the pseudo-second-order model were found close to those determined experimentally. Based on the above findings, one may conclude that the pseudo-second-order kinetic representation is more adequate for describing the adsorption kinetics of TY onto the adsorbents, which implies that the adsorption of TY by NiAl-HT, CoAl-HT, and NiCoAl-HT corresponds to chemisorptions [8].

Table 4. Kinetic parameters of the pseudo-first-order, pseudo-second-order, and the intra-particle diffusion models for the adsorption of TY onto NiAl-HT, CoAl-HT, and NiCoAl-HT.

Parameters	NiAl-HT	CoAL-HT	NiCoAl-HT
pseudo-first-order model			
$Q_{e,exp}$ ($mg{\cdot}g^{-1}$)	29.299	20.814	24.303
K_1 (min^{-1})	0.335 ± 0.030	0.402 ± 0.059	0.036 ± 0.007

Table 4. *Cont.*

Parameters	NiAl-HT	CoAL-HT	NiCoAl-HT
$Q_{e,cal}$ ($mg \cdot g^{-1}$)	29.299 ± 0.227	19.825 ± 0.206	24.343 ± 1.717
R^2	0.985	0.974	0.715
RMSE	0.852	0.783	3.245
MSE	0.726	0.613	10.528
pseudo-second-order model			
$Q_{e,exp}$ ($mg \cdot g^{-1}$)	29.299	20.814	24.303
K_2 ($g \cdot mg^{-1} \cdot min^{-1}$)	0.0369 ± 0.003	0.0448 ± 0.007	0.0043 ± 0.0006
$Q_{e,cal}$ ($mg \cdot g^{-1}$)	29.607 ± 0.103	20.461 ± 0.157	25.115 ± 0.644
R^2	0.998	0.992	0.965
RMSE	0.292	0.437	1.132
MSE	0.085	0.191	1.281
Intraparticle diffusion model			
K_{int} ($mg \cdot g^{-1} \cdot min^{-1}$)	1.149 ± 0.421	0.864 ± 0.277	1.534 ± 0.204
C ($mg \cdot g^{-1}$)	19.372 ± 3.112	12.810 ± 2.051	8.306 ± 1.508
R^2	0.287	0.353	0.776
RMSE	5.929	3.907	2.873
MSE	35.159	15.266	8.257

3.2.6. Adsorption Equilibrium Isotherms

The adsorption isotherm expresses the relationship between the adsorbate concentration and its degree of accumulation on the adsorbent surface. The study was carried out with optimized masses (80 mg) of the materials (NiAl-HT, CoAl-HT NiCoAl-HT) in 20 mL of the aqueous solution with specific dye concentration. The experiments were carried out at room temperature, with an initial solution concentration varying between 50 and 400 $mg \cdot L^{-1}$; the initial pH of the dye solution was unchanged (pH 3). The prepared suspensions were first shaken for 180 min to reach equilibrium. Then they were centrifuged and characterized.

The resulting adsorption isotherm could be fitted using the Langmuir (Equations (11) and (12)) and Freundlich (Equations (13)) adsorption isotherm models as a nonlinear expression.

$$Q_e = Q_{max} \times \frac{K_L C_e}{1 + K_L C_e} \tag{11}$$

where Q_{max} ($mg \cdot g^{-1}$) and K_L ($L \cdot mg^{-1}$) are Langmuir parameters; they are related to the maximum adsorption capacity and the Langmuir constant, respectively.

The dimensionless separation factor [54] is expressed as following Equation (12):

$$R_L = \frac{1}{1 + K_L C_0} \tag{12}$$

where C_0 is the highest initial concentration ($mg \cdot L^{-1}$)

$$Q_e = K_F \times C_e^{\frac{1}{n}} \tag{13}$$

where K_F ($mg \cdot g^{-1}$) $(L \cdot mg^{-1})^{1/n}$ and n are Freundlich parameters; they are associated with the adsorption capacity and the sorption intensity, respectively. The equilibrium parameters for the adsorption of TY dye by the adsorbents NiAl-HT, CoAl-HT, and NiCoAl-HT are summarized in Table 5.

Table 5. Langmuir and Freundlich isotherm parameters for the adsorption of TY on adsorbents NiAl-HT, CoAL-HT, and NiCoAl-HT.

Parameters	NiAl-HT	CoAL-HT	NiCoAl-HT
Langmuir			
$\mathbf{Q_{max}(mg{\cdot}g^{-1})}$	234.245 ± 29.722	55.369 ± 2.542	152.511 ± 17.595
$\mathbf{K_L}$	0.009 ± 0.002	0.028 ± 0.005	0.027 ± 0.008
$\mathbf{R_L}$	0.217	0.082	0.084
$\mathbf{R^2}$	0.954	0.954	0.867
RMSE	11.171	2.618	15.099
MSE	124.781	6.856	227.993
Freundlich			
$\mathbf{K_F}$	7.893 ± 3.537	9.319 ± 2.334	18.307 ± 7.474
n	1.784 ± 0.296	3.270 ± 0.539	2.72 ± 0.651
$\mathbf{R^2}$	0.881	0.884	0.738
RMSE	18.045	4157	21.214
MSE	325.627	17.283	450.053

Considering the high values of R^2 and small values of RMSE and MSE that are given in Table 5, it can be stated that the Langmuir model (Figure 10) represents the best fit for the experimental adsorption data as compared with the Freundlich model. One can also observe that the values of the dimensionless constant, also called separation factor, R_L are within the interval extending from 0 to 1 ($0 < R_L < 1$), which confirms the existence of a good monolayer adsorption [39]. The adsorption capacity (Q_{max}) values for the adsorbents NiAl-HT, CoAl-HT, and NiCoAl-HT were found, respectively, equal to 234.245 $mg{\cdot}g^{-1}$, 55.369 $mg{\cdot}g^{-1}$, and 152.511 $mg{\cdot}g^{-1}$. Note also that the adsorption capacities decreased in the following order: NiAl-HT > NiCoAl-HT > CoAl-HT, which is corroborated by the decreasing interlamellar distance (Table 2).

3.2.7. Adsorption Thermodynamics

Furthermore, thermodynamic parameters, such as the change in Gibbs free energy ΔG° ($KJ{\cdot}mol^{-1}$), as well as the enthalpy change ΔH° ($KJ{\cdot}mol^{-1}$) and entropy change ΔS° ($KJ{\cdot}mol^{-1}{\cdot}K^{-1}$), at constant temperature (K), is expressed by the Equations given below.

$$K_d = \frac{Q_e}{C_e}$$

$$\Delta G^\circ = -RTln\ K_d = \Delta H^\circ - T\Delta S^\circ$$

$$lnK_d = \left(\frac{\Delta S^\circ}{R}\right) - \left(\frac{\Delta H^\circ}{R}\right)\frac{1}{T} = -\frac{\Delta G^\circ}{RT}$$

where K_d ($mL{\cdot}g^{-1}$) is the distribution constant, C_e ($mg{\cdot}L^{-1}$) is the equilibrium concentration in solution, Q_e ($mg{\cdot}L^{-1}$) is the amount of adsorbed dye at equilibrium, T is the temperature (K) [298–328], and R is the universal gas constant (8.314 J mol^{-1} K^{-1}). The values of ΔH° and ΔS° were determined from the slope and the intercept of the plot of ln K_d versus 1/T, as shown in Figure 11b.

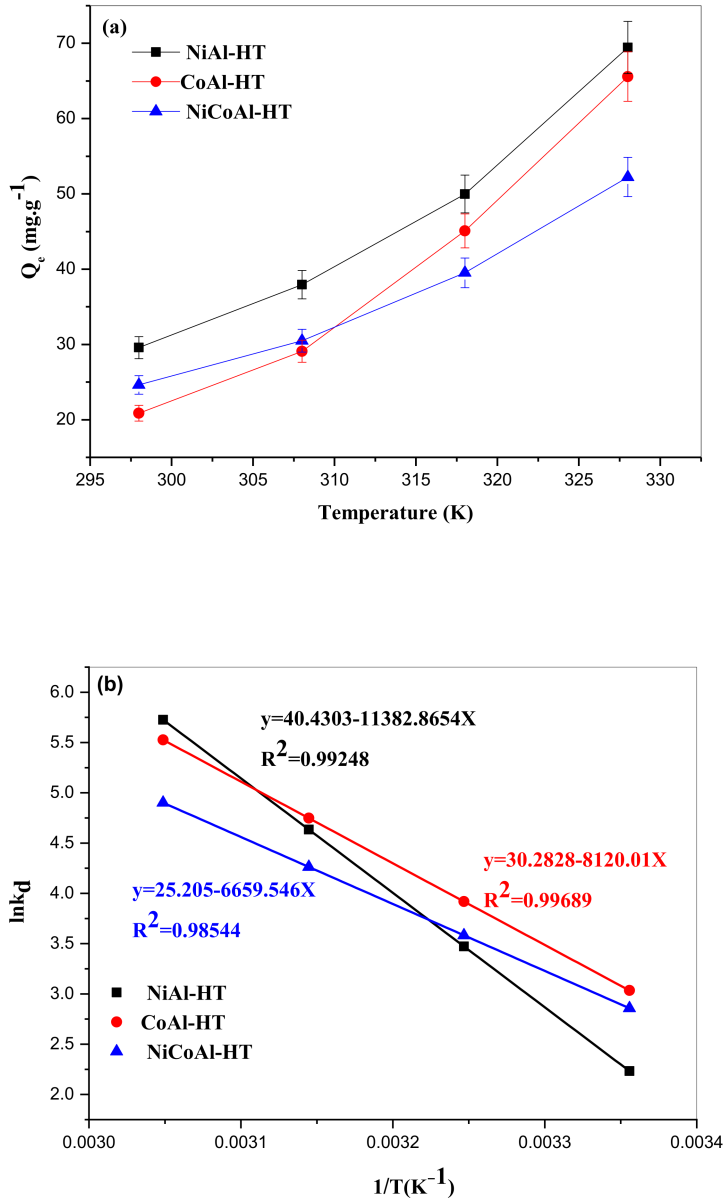

Figure 11. (**a**) Impact of temperature on TY uptake onto NiAl-HT, CoAl-HT, and NiCoAl-HT (C_0 = 100 mg·L^{-1}, m = 80 mg, V = 20 mL, pH 3); (**b**) Evolution of LnK_d as function of 1/T.

The thermodynamic parameters for the sorption of TY on sorbents NiAl-HT, CoAl-HT, and NiCoAl-HT are reported in Table 6. It should be noted that the negative values of ΔG° confirm the feasibility of the adsorption process and the spontaneous nature of the sorption of TY onto NiAl-HT, CoAl-HT, and NiCoAl-HT, whereas the positive values of ΔH° confirm that the adsorption process is endothermic, which enhances the adsorption rate as the temperature rises. Similarly, the positive value of Δ*S*° implies an increase in the stochastic distribution at the solid–liquid interface through the adsorption of TY on NiAl-HT, CoAl-HT, and NiCoAl-HT [55]. On the other side, it was observed that the value ΔG° goes down when the temperature increases, which induces that adsorption is more favorable at high temperatures [39].

Table 6. Thermodynamic parameters for the adsorption of TY onto NiAl-HT, CoAl-HT, and NiCoAl-HT.

Parameters	T (K)	ΔG° (KJ·mol^{-1})	ΔH° (KJ·mol^{-1})	ΔS° (KJ·mol^{-1}·K^{-1})
NiAl-HT	298	−5.532	94.637	0.34
	308	−8.893		
	318	−12.255		
	328	−15.616		
CoAl-HT	298	−7.518	67.509	0.25
	308	−10.036		
	318	−12.553		
	328	−15.071		
NiCoAl-HT	298	−7.079	55.367	0.21
	308	−9.175		
	318	−11.271		
	328	−13.366		

4. Conclusions

In this paper, work focuses on studying the removal of Titan Yellow (TY) dye, which is a water pollutant using three matrices of layered double hydroxide materials (LDHs; M^{+2}Al-HT), with M^{2+} = Ni, Co, or NiCo prepared by **a** co-precipitation method at constant pH. The characterization of these materials by the XRD analysis technique showed that these are indeed double lamellar hydroxides, as has been reported in the literature, with an interlamellar distance that follows the following order: NiAl-HT > NiCoAl-HT > CoAl-HT. Furthermore, the Fourier-transform infrared spectroscopy (FTIR) technique was used, before and after adsorption, to confirm the presence of vibration bands of the dye that is expected to be eliminated. Moreover, the TG/DTG method made it possible to show that the decarbonation temperature of the compounds NiAl-HT, CoAl-HT, and NiCoAl-HT were equal to 353 °C, 280 °C, and 377 °C, respectively. In addition, it was found that the BET specific surface area of NiAl-HT is higher than those of NiCoAl-HT and CoAl-HT, and the SEM-EDX results confirm the creation of the hydrotalcite type material.

The adsorption of Titan Yellow (TY) reached equilibrium after 40 min, 90 min, and 120 min for NiAl-HT, CoAl-HT, and NiCoAl-HT, respectively. With regard to the adsorption kinetics, it was shown that it is best described by the pseudo-second order kinetic nonlinear model. In addition, it was found that the amount of adsorbed pollutant was optimal for a pH equal to 3. The findings of this study are better described by Langmuir's model, and the adsorbents used exhibited a high adsorption capacity, that is, 234.245 mg·g^{-1}, 152.511 mg·g^{-1}, and 55.369 mg·g^{-1} for NiAl-HT, NiCoAl-HT, and CoAl-HT, respectively. These findings imply that NiAl-HT is the best adsorbent of TY. As for the thermodynamic analysis, it showed that the sorption augmented when the temperature went up from 298 K to 328 K. Finally, it was found that the sorption process is spontaneous and endothermic.

In general, we could conclude that the adsorbents studied here could be successfully applied in the cleaning of the wastewaters of the dyeing industry, and these findings imply that NiAl-HT is the best adsorbent of TY and it can be used in the future in the field of catalysis.

Author Contributions: Conceptualization, S.C. (Samira Chouikh), S.C. (Sabrina Cheikh) and A.I.; Methodology, S.C. (Samira Chouikh), S.C. (Sabrina Cheikh), A.I., L.M., A.A. and N.B.; Software, S.C. (Samira Chouikh); Validation, L.M., A.A. and N.B.; Formal analysis, A.I., L.M., A.A. and A.B.; Investigation, S.C. (Samira Chouikh); Resources, A.B., A.A. and L.M.; Data curation S.C. (Samira Chouikh), S.C. (Sabrina Cheikh) and A.I.; Writing—original draft preparation, S.C. (Samira Chouikh), S.C. (Sabrina Cheikh) and A.I.; Writing—review and editing, S.C. (Samira Chouikh), S.C. (Sabrina Cheikh), A.I., A.B., A.A., L.M. and N.B.; Visualization, A.A., A.B., A.I. and L.M.; Supervision, A.A., L.M. and A.B.; Project administration, A.B., A.A. and L.M. All authors have read and agreed to the published version of the manuscript.

Funding: This research received no external funding.

Institutional Review Board Statement: Not applicable.

Informed Consent Statement: Not applicable.

Data Availability Statement: Not applicable.

Acknowledgments: The authors wish to thank all who assisted in conducting this work.

Conflicts of Interest: The authors declare no conflict of interest.

References

1. Owa, F.D. Water Pollution: Sources, Effects, Control and Management. *Mediterr. J. Soc. Sci.* **2013**, *4*, 65. [CrossRef]
2. Jayaswal, K.; Sahu, V.; Gurjar, B. Water Pollution, Human Health and Remediation. In *Water Remediation. Energy, Environment, and Sustainability*; Springer: Singapore, 2018; pp. 11–27. ISBN 978-981-10-7550-6.
3. Chedri Mammar, A.; Mouni, L.; Bollinger, J.-C.; Belkhiri, L.; Bouzaza, A.; Assadi, A.A.; Belkacemi, H. Modeling and Optimization of Process Parameters in Elucidating the Adsorption Mechanism of Gallic Acid on Activated Carbon Prepared from Date Stones. *Sep. Sci. Technol.* **2020**, *55*, 3113–3125. [CrossRef]
4. Khattab, T.; Abdelrahman, M.; Rehan, M. Textile Dyeing Industry: Environmental Impacts and Remediation. *Environ. Sci. Pollut. Res.* **2020**, *27*, 3803–3818. [CrossRef] [PubMed]
5. El-Azazy, M.; Dimassi, S.; El-Shafie, A.; Issa, A. Bio-Waste Aloe Vera Leaves as an Efficient Adsorbent for Titan Yellow from Wastewater: Structuring of a Novel Adsorbent Using Plackett-Burman Factorial Design. *Appl. Sci.* **2019**, *9*, 4856. [CrossRef]
6. Haque, M.M.; Haque, M.A.; Mosharaf, M.K.; Marcus, P. Decolorization, Degradation and Detoxification of Carcinogenic Sulfonated Azo Dye Methyl Orange by Newly Developed Biofilm Consortia. *Saudi J. Biol. Sci.* **2020**, *28*, 793–804. [CrossRef]
7. Fenelon, E.; Ni'am, A.; Wang, Y.-F.; You, S.-J. Study of the Potential of La/Bi2S3 Catalyst for Photodegradation of Acid Yellow 42 Dye under Visible Light. *J. Nanomater.* **2022**, *2022*, 2990466. [CrossRef]
8. Shi, Q.-X.; Li, Y.; Wang, L.; Wang, J.; Cao, Y.-L. Preparation of Supported Chitosan Adsorbent with High Adsorption Capacity for Titan Yellow Removal. *Int. J. Biol. Macromol.* **2020**, *152*, 449–455. [CrossRef]
9. Dadou, S.; Berrama, T.; Doufene, N.; Zekkaoui, C.; Beriber, A. Evaluating Untreated Clay's Adsorptive Capacity to Remove an Anionic Dye from Aqueous Solution. *Arab. J. Sci. Eng.* **2019**, *44*, 9889–9903. [CrossRef]
10. Hadadi, A.; Imessaoudene, A.; Bollinger, J.-C.; Cheikh, S.; Assadi, A.A.; Amrane, A.; Kebir, M.; Mouni, L. Parametrical Study for the Effective Removal of Mordant Black 11 from Synthetic Solutions: Moringa Oleifera Seeds' Extracts Versus Alum. *Water* **2022**, *14*, 4109. [CrossRef]
11. BinSabt, M.; Sagar, V.; Singh, J.; Rawat, M.; Shaban, M. Green Synthesis of CS-TiO2 NPs for Efficient Photocatalytic Degradation of Methylene Blue Dye. *Polymers* **2022**, *14*, 2677. [CrossRef]
12. Bhad, R.M.; Das, A.; Kodape, S.M. Ozonation of Procion Blue Reactive Dye and Its Kinetics Study. *Pollution* **2022**, *8*, 529–541. [CrossRef]
13. Vecino, X.; Reig, M. Wastewater Treatment by Adsorption and/or Ion-Exchange Processes for Resource Recovery. *Water* **2022**, *14*, 911. [CrossRef]
14. Nidheesh, P.V.; Couras, C.; Karim, A.V.; Nadais, H. A Review of Integrated Advanced Oxidation Processes and Biological Processes for Organic Pollutant Removal. *Chem. Eng. Commun.* **2021**, *209*, 390–432. [CrossRef]
15. Abd Malek, N.; Jawad, A.H.; Ismail, K.; Razuan, R.; Alothman, Z. Fly Ash Modified Magnetic Chitosan-Polyvinyl Alcohol Blend for Reactive Orange 16 Dye Removal: Adsorption Parametric Optimization. *Int. J. Biol. Macromol.* **2021**, *189*, 464–476. [CrossRef]
16. Liu, F.; Hua, S.; Wang, C.; Qiu, M.; Jin, L.; Hu, B. Adsorption and Reduction of Cr(VI) from Aqueous Solution Using Cost-Effective Caffeic Acid Functionalized Corn Starch. *Chemosphere* **2021**, *279*, 130539. [CrossRef]
17. Bekhoukh, A.; Moulefera, I.; Zeggai, F.Z.; Benyoucef, A.; Bachari, K. Anionic Methyl Orange Removal from Aqueous Solutions by Activated Carbon Reinforced Conducting Polyaniline as Adsorbent: Synthesis, Characterization, Adsorption Behavior, Regeneration and Kinetics Study. *J. Polym. Environ.* **2022**, *30*, 886–895. [CrossRef]
18. Sarabadan, M.; Bashiri, H.; Mousavi, S. Adsorption of Crystal Violet Dye by Zeolite-Montmorillonite: Modeling, Kinetic and Equilibrium Studies. *Clay Miner.* **2019**, *54*, 357–368. [CrossRef]
19. Wang, X.; Pfeiffer, H.; Wei, J.; Dan, J.; Wang, J.; Zhang, J. 3D Porous Ca-Modified Mg-Zr Mixed Metal Oxide for Fluoride Adsorption. *Chem. Eng. J.* **2021**, *428*, 131371. [CrossRef]
20. Junejo, R.; Memon, S.; Memon, F.; Memon, A.; Durmaz, F.; Bhatti, A.; Bhatti, A. Thermodynamic and Kinetic Studies for Adsorption of Reactive Blue (RB-19) Dye Using Calix[4]Arene-Based Adsorbent. *J. Chem. Eng. Data* **2019**, *64*, 3407–3415. [CrossRef]
21. Bouchelkia, N.; Tahraoui, H.; Amrane, A.; Belkacemi, H.; Bollinger, J.-C.; Bouzaza, A.; Zoukel, A.; Zhang, J.; Mouni, L. Jujube Stones Based Highly Efficient Activated Carbon for Methylene Blue Adsorption: Kinetics and Isotherms Modeling, Thermodynamics and Mechanism Study, Optimization via Response Surface Methodology and Machine Learning Approaches. *Process Saf. Environ. Prot.* **2022**, *170*, 513–535. [CrossRef]

22. Sabrina, C.; Imessaoudene, A.; Bollinger, J.-C.; Hadadi, A.; Manseri, A.; Bouzaza, A.; Assadi, A.; Amrane, A.; Zamouche, M.; Jery, A.; et al. Complete Elimination of the Ciprofloxacin Antibiotic from Water by the Combination of Adsorption-Photocatalysis Process Using Natural Hydroxyapatite and TiO_2. *Catalysts* **2023**, *13*, 336. [CrossRef]
23. Shah, A.K.; Ali, Z.M.; Laghari, A.; Farman, S.; Shah, S.F.; Kazi, D. Utilization of Fly Ash as Low-Cost Adsorbent for the Treatment of Industrial Dyes Effluents—A Comparative Study. *Res. Rev. J. Eng. Technol.* **2013**, *2*, 1–10.
24. Lim, L.; Priyantha, N.; Chan, C.; Matassan, D.; Hei Ing, C.; Kooh, M.R.R. Adsorption Behavior of Methyl Violet 2B Using Duckweed: Equilibrium and Kinetics Studies. *Arab. J. Sci. Eng.* **2014**, *39*, 6757–6765. [CrossRef]
25. Kooh, M.R.R.; Dahri, M.K.; Lim, L.; Lim, L.-H. Batch Adsorption Studies on the Removal of Acid Blue 25 from Aqueous Solution Using Azolla Pinnata and Soya Bean Waste. *Arab. J. Sci. Eng.* **2016**, *41*, 2453–2464. [CrossRef]
26. Lu, Y.; Kooh, M.R.R.; Lim, L.; Priyantha, N. Effective and Simple NaOH-Modification Method to Remove Methyl Violet Dye via Ipomoea Aquatica Roots. *Adsorpt. Sci. Technol.* **2021**, *2021*, 5932222. [CrossRef]
27. Lim, L.; Priyantha, N.; Mansor, N. *Artocarpus Altilis* (Breadfruit) Skin as a Potential Low-Cost Biosorbent for the Removal of Crystal Violet Dye: Equilibrium, Thermodynamics and Kinetics Studies. *Environ. Earth Sci.* **2014**, *73*, 3239–3247. [CrossRef]
28. Zaidi, N.; Lim, L.; Usman, A.; Kooh, M.R.R. Efficient Adsorption of Malachite Green Dye Using Artocarpus Odoratissimus Leaves with Artificial Neural Network Modelling. *Desalination Water Treat.* **2018**, *101*, 313–324. [CrossRef]
29. Gama, B.M.V.d.; Selvasembian, R.; Giannakoudakis, D.A.; Triantafyllidis, K.S.; McKay, G.; Meili, L. Layered Double Hydroxides as Rising-Star Adsorbents for Water Purification: A Brief Discussion. *Molecules* **2022**, *27*, 4900. [CrossRef]
30. El Hassani, K.; Beakou, B.; Kalnina, D.; Oukani, E.; Anouar, A. Effect of Morphological Properties of Layered Double Hydroxides on Adsorption of Azo Dye Methyl Orange: A Comparative Study. *Appl. Clay Sci.* **2017**, *140*, 124–131. [CrossRef]
31. Hidouri, S.; Errachid, A.; Baussels, J.; Korpan, Y.; Ruiz-Sanchez, O.; Baccar, Z. Potentiometric Sensing of Histamine Using Immobilized Enzymes on Layered Double Hydroxides. *J. Food Sci. Technol. Mysore* **2020**, *58*, 2936–2942. [CrossRef]
32. Fatima, K.; EZZIANE, K.; Bahmani, A.; Nourredine, B.; Mayouf, S. Evans Blue Dye Removal from Contaminated Water on Calcined and Uncalcined Cu-Al-CO_3 Layered Double Hydroxide Materials Prepared by Coprecipitation. *Bull. Mater. Sci.* **2019**, *42*, 14. [CrossRef]
33. Vaccari, A. Layered Double Hydroxides: Present and Future: V. Rives (Ed.), Nova Science Publishers, Inc., New York, 2001, IX+439 Pp., ISBN 1-59033-060-9. *Appl. Clay Sci.* **2002**, *22*, 75–76. [CrossRef]
34. Santos, R.M.M.D.; Gonçalves, R.G.L.; Constantino, V.R.L.; Santilli, C.V.; Borges, P.D.; Tronto, J.; Pinto, F.G. Adsorption of Acid Yellow 42 Dye on Calcined Layered Double Hydroxide: Effect of Time, Concentration, PH and Temperature. *Appl. Clay Sci.* **2017**, *140*, 132–139. [CrossRef]
35. Malak-Polaczyk, A.; Vix-Guterl, C.; Frackowiak, E. Carbon/Layered Double Hydroxide (LDH) Composites for Supercapacitor Application. *Energy Fuels* **2010**, *24*, 3346–3351. [CrossRef]
36. Sudare, T.; Tamura, S.; Tanaka, H.; Hayashi, F.; Teshima, K. Highly Crystalline Ni–Co Layered Double Hydroxide Fabricated via Topochemical Transformation with a High Adsorption Capacity for Nitrate Ions. *Inorg. Chem.* **2019**, *58*, 15710–15719. [CrossRef]
37. Ali, B.; Benhadria, N.; Abdelkader, E.; Karima, E.; Nourredine, B. Competitive Adsorption of Binary Dye from Aqueous Solutions Using Calcined Layered Double Hydroxides. *Int. J. Environ. Anal. Chem.* **2020**, *102*, 1–20. [CrossRef]
38. Bouteraa, S.; Saiah, F.B.D.; Hamouda, S.; Bettahar, N. Zn-M-CO_3 Layered Double Hydroxides (M = Fe, Cr, or Al): Synthesis, Characterization, and Removal of Aqueous Indigo Carmine. *Bull. Chem. React. Eng. Catal.* **2020**, *15*, 43–54. [CrossRef]
39. Rezak, N.; Bahmani, A.; Bettahar, N. Adsorptive Removal of P(V) and Cr(VI) by Calcined Zn-Al-Fe Ternary LDHs. *Water Sci. Technol.* **2021**, *83*, 2504–2517. [CrossRef]
40. Santosa, S.; Krisbiantoro, P.; Astuti, D. Reusable High Performance of Calcined Mg/Al Hydrotalcite for the Removal of Navy Blue and Yellow F3G Dyes. *Chin. J. Chem. Eng.* **2020**, *38*, 247–254. [CrossRef]
41. Amin, M.; Alazba, P.; Shafiq, M. LDH of NiZnFe and Its Composites with Carbon Nanotubes and Data-Palm Biochar with Efficient Adsorption Capacity for RB5 Dye from Aqueous Solutions: Isotherm, Kinetic, and Thermodynamics Studies. *Curr. Appl. Phys.* **2020**, *40*, 90–100. [CrossRef]
42. Bardestani, R.; Patience, G.; Kaliaguine, S. Experimental Methods in Chemical Engineering: Specific Surface Area and Pore Size Distribution Measurements—BET, BJH, DFT. *Can. J. Chem. Eng.* **2019**, *97*, 2781–2791. [CrossRef]
43. Imessaoudene, A.; Sabrina, C.; Bollinger, J.-C.; Belkhiri, L.; Tiri, A.; Bouzaza, A.; Jery, A.; Amrane, A.; Mouni, L. Zeolite Waste Characterization and Use as Low-Cost, Ecofriendly, and Sustainable Material for Malachite Green and Methylene Blue Dyes Removal: Box–Behnken Design, Kinetics, and Thermodynamics. *Appl. Sci.* **2022**, *12*, 7587. [CrossRef]
44. Djezar, H.; Rida, K.; Salhi, M. Efficient Adsorbent for the Removal of Methyl Orange and Congo Red by Calcined Zn-Al Layered Double Hydroxide. *Inorg. Nano-Met. Chem.* **2021**, *52*, 161–172. [CrossRef]
45. Sun, S.; Jin, X.; Cong, B.; Zhou, X.; Hong, W.; Chen, G. Construction of Porous Nanoscale NiO/$NiCo_2O_4$ Heterostructure for Highly Enhanced Electrocatalytic Oxygen Evolution Activity. *J. Catal.* **2019**, *379*, 1–9. [CrossRef]
46. Abdellaoui, K.; Pavlovic, I.; Bouhent, M.; Benhamou, A.; Barriga, C. A comparative study of the amaranth azo dye adsorption/desorption from aqueous solutions by layered double hydroxides. *Appl. Clay Sci.* **2017**, *143*, 142–150. [CrossRef]
47. Rivera, J.A.; Fetter, G.; Jiménez, Y.; Xochipa, M.M.; Bosch, P. Nickel Distribution in (Ni, Mg)/Al-Layered Double Hydroxides. *Appl. Catal. A Gen.* **2007**, *316*, 207–211. [CrossRef]
48. Auxilio, A.; Andrews, P.; Junk, P.; Spiccia, L.; Neumann, D.; Vanderhoek, N. Adsorption and Intercalation of Acid Blue 9 on Mg–Al Layered Double Hydroxides of Variable Metal Composition. *Polyhedron* **2007**, *26*, 3479–3490. [CrossRef]

49. Khenifi, A.; Derriche, Z.; Mousty, C.; Prévot, V.; Forano, C. Adsorption of Glyphosate and Glufosinate by Ni_2AlNO_3 Layered Double Hydroxide. *Appl. Clay Sci.* **2010**, *47*, 362–371. [CrossRef]
50. El Hassan, E.; Lakraimi, M.; Badreddine, M.; Legrouri, A.; Cherkaoui, O.; Berraho, M. Removal of Remazol Blue 19 from Wastewater by Zinc–Aluminium–Chloride-Layered Double Hydroxides. *Appl. Water Sci.* **2014**, *3*, 431–438. [CrossRef]
51. Thommes, M.; Kaneko, K.; Neimark, A.V.; Olivier, J.P.; Rodriguez-Reinoso, F.; Rouquerol, J.; Sing, K.S.W. Physisorption of Gases, with Special Reference to the Evaluation of Surface Area and Pore Size Distribution (IUPAC Technical Report). *Pure Appl. Chem.* **2015**, *87*, 1051–1069. [CrossRef]
52. Lazaridis, N.K.; Karapantsios, T.D.; Georgantas, D. Kinetic Analysis for the Removal of a Reactive Dye from Aqueous Solution onto Hydrotalcite by Adsorption. *Water Res.* **2003**, *37*, 3023–3033. [CrossRef]
53. Imessaoudene, A.; Sabrina, C.; Hadadi, A.; Nadia, H.; Bollinger, J.-C.; Amrane, A.; Tahraoui, H.; Manseri, A.; Mouni, L. Adsorption Performance of Zeolite for the Removal of Congo Red Dye: Factorial Design Experiments, Kinetic, and Equilibrium Studies. *Separations* **2023**, *10*, 57. [CrossRef]
54. Giles, C.H.; MacEwan, T.H.; Nakhwa, S.N.; Smith, D. Studies in Adsorption Part XI: A System of Classification of Solution Adsorption Isotherms and Its Use in Diagnosis of Adsorption Mechanism and Measurement of Specific Surface Areas of Solid. *J. Chem. Soc. (Resumed)* **1960**, *111*, 3973. [CrossRef]
55. Rastgordani, M.; Zolgharnein, J.; Mahadavi, V. Derivative Spectrophotometry and Multivariate Optimization for Simultaneous Removal of Titan Yellow and Bromophenol Blue Dyes Using Polyaniline@SiO_2 Nanocomposite. *Microchem. J.* **2020**, *155*, 104717. [CrossRef]

Disclaimer/Publisher's Note: The statements, opinions and data contained in all publications are solely those of the individual author(s) and contributor(s) and not of MDPI and/or the editor(s). MDPI and/or the editor(s) disclaim responsibility for any injury to people or property resulting from any ideas, methods, instructions or products referred to in the content.